PHILOSOPHICAL TRANSACTIONS OF THE ROYAL SOCIETY A

Phil. Trans. R. Soc. A (2011) **369**, 3658–3678
doi:10.1098/rsta.2011.0190

Spin control by application of electric current and voltage in FeCo–MgO junctions

By Yoshishige Suzuki[1,2,3,*], Hitoshi Kubota[2,3], Ashwin Tulapurkar[1,†] and Takayuki Nozaki[1,3]

[1] *Graduate School of Engineering Science, Osaka University, Toyonaka, Osaka 560-8531, Japan*
[2] *Nanoelectronics Research Institute (NeRI), National Institute of Advanced Industrial Science and Technology (AIST), Tsukuba, Ibaraki 305-8568, Japan*
[3] *Core Research for Evolutional Science and Technology (CREST), Saitama 332-0012, Japan*

Efficient control and detection of spins are the most important tasks in spintronics. The current and voltage applied to a magnetic tunnel junction may exert a torque on the magnetic thin layer in the junction and cause its reversal or continuous precession. The discovery of the giant tunnelling magnetoresistance effect in ferromagnetic tunnelling junctions using an MgO barrier enabled us to obtain a large signal output from the magnetization reversal and precession. Also, the interplay of large spin configuration–electric conduction coupling provides highly nonlinear effects like the spin-torque diode effect. The negative resistance effect and amplification using it are predicted. A new discovery about a voltage-induced magnetic anisotropy change in Fe ultrathin films is also discussed.

Keywords: electric current; voltage; spintronics

1. Tunnelling magnetoresistance effect

Efficient control and detection of spins are the most important issues in spintronics. The discovery of the giant magnetoresistance effect in ferromagnetic metallic multi-layers [1] and the tunnelling magnetoresistance effect in magnetic tunnel junctions (MTJs) using an Al–O barrier [2,3] enabled the effective detection of magnetization in nanoscale magnetic cells. In figure 1, a schematic of an MTJ is shown. The MTJ consists of two ferromagnetic layers (e.g. CoFeB) separated by an insulating barrier layer. The electrical conductance, G, of the junction varies with the relative angle, θ, between the two magnetization directions as [4]

$$G(\theta) = \frac{G_{\mathrm{P}} + G_{\mathrm{AP}}}{2} + \frac{G_{\mathrm{P}} - G_{\mathrm{AP}}}{2} \cos\theta. \tag{1.1}$$

*Author for correspondence (suzuki-y@mp.es.osaka-u.ac.jp).
†Present address: Indian Institute of Technology, Powai, Mumbai 400076, India.

One contribution of 10 to a Discussion Meeting Issue ‘The spin on electronics’.

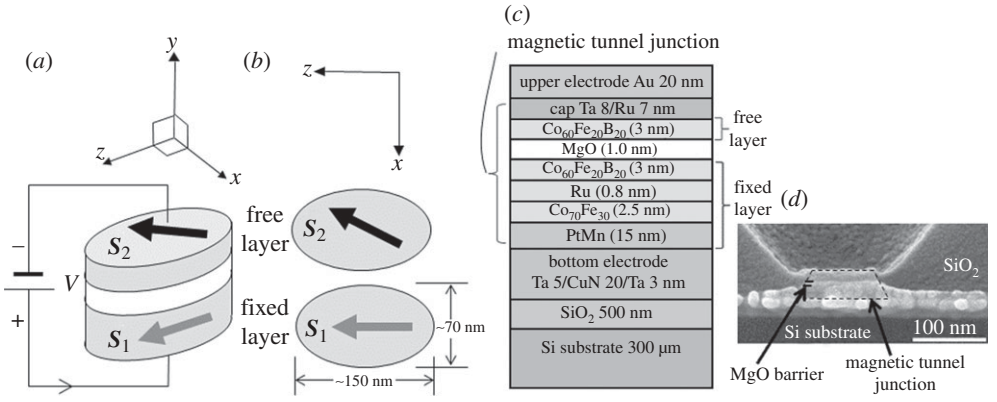

Figure 1. Typical structure of a magnetic tunnel junction (MTJ) nanopillar designed for spin-injection magnetization switching (SIMS) experiments. (*a*) In the bird's eye view, the upper magnetic layer acts as a magnetically free layer, whereas lower magnetic layers are thicker than the free layer and act as a spin polarizer. The spins in the lower layer are usually pinned by an exchange interaction at the bottom interface to an antiferromagnetic material. Therefore, the spin polarizer layer is often called the pinned, fixed or reference layer. In MTJ nanopillars, the layer between the two ferromagnetic layers is made of an insulator such as MgO. (*b*) Top view of the junction, which has an elliptical shape with a diameter of around 100 nm. (*c*) The actual stack structure of the MTJ. A magnetic multi-layer including the tunnelling barrier is deposited under vacuum by a sputtering method. The free layer is typically a few nanometres thick. (*d*) Cross-sectional image of a typical MTJ. The image was taken for a cleaved cross-section of the MTJ using a scanning electron microscope (SEM) operated at 5 kV.

Here, G_{P} and G_{AP} are the conductance for parallel ($\theta = 0$) and anti-parallel ($\theta = \pi$) configurations of the magnetizations, respectively. The magnetoresistance ratio (MR) is usually defined as the ratio of the conductance change to the conductance in the anti-parallel configuration:

$$\mathrm{MR} = \frac{G_{\mathrm{P}} - G_{\mathrm{AP}}}{G_{\mathrm{AP}}} \times 100(\%). \tag{1.2}$$

The maximum MR was thought to be around 70 per cent for 3d transition metal/Al–O MTJs because of the limited spin polarization of the conduction electrons at the Fermi energy in the 3d ferromagnetic transition metals. MTJs using an MgO barrier, however, had overcome this limitation [5–7] by virtue of their band selectivity and are now offering more than 1000 per cent MR at room temperature (RT) [8].

In this paper, we show that 3d transition metal/MgO barrier junctions also offer effective methods to control the magnetization direction by the application of either current or voltage.

2. Spin-injection magnetization switching

The electric current-induced spin-transfer torque was first predicted theoretically [9,10] and subsequently observed experimentally in metallic nanojunctions as an excitation of spin waves [11] and as a spin-injection magnetization switching

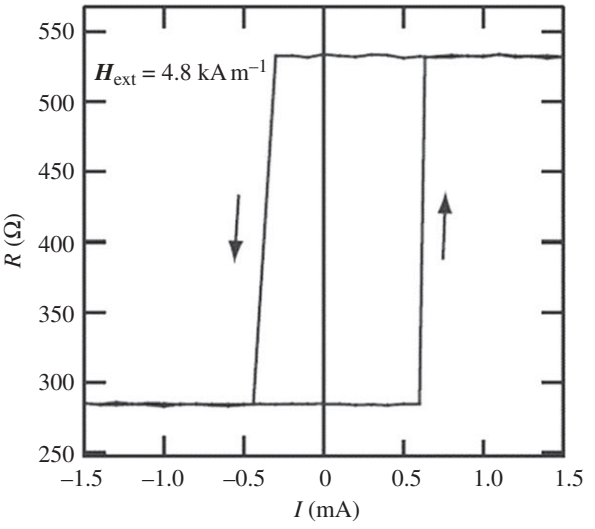

Figure 2. Typical SIMS hysteresis loop obtained for a CoFeB/MgO/CoFeB MTJ. The junction area, free-layer thickness, resistance × area product and MR are 100 × 200 nm, 3 nm, 3 Ω μm^2 and about 100 per cent, respectively. Measurements were performed at RT using electric current pulses of $t_p = 100$ ms duration. The resistance of the junction was measured after each pulse to avoid the effect of heating on the sample resistance.

(SIMS) [12]. Later, SIMS was also observed in Al–O barrier MTJs [13] and in MgO barrier MTJs [14,15]. In figure 2, typical resistance–current hysteresis in a CoFeB/MgO/CoFeB MTJ [14] is shown. Magnetization switchings between parallel (P) and anti-parallel (AP) states were observed as resistance changes owing to the MR effect in the MTJ. The sample was made by sputter deposition and successive ion milling, metallization and annealing processes [14]. The lateral shape of the MTJ pillar was elliptical, with dimensions of about 200 × 100 nm. The angular momentum in the fixed layer, $\boldsymbol{S}_1$, is fixed along the major axis of the ellipse through an exchange interaction with the antiferromagnetic layer made of PtMn. Without current injection, the angular momentum in the free layer, $\boldsymbol{S}_2$, also lies along the major axis of the ellipse, because of magnetostatic shape anisotropy, and is in either a parallel (P) or anti-parallel (AP) state with respect to $\boldsymbol{S}_1$. To give an asymmetry with respect to the current direction, the thickness of the free layer is smaller than that of the fixed layer. The current was applied as a series of 100 ms wide pulses. In between the pulses, the sample resistance was measured to check the magnetization configuration while the pulse height was swept between −1.5 and +1.5 mA. For the data shown in figure 2, the hysteresis measurement started at zero pulse height for the P state (285 Ω). An increase in pulse height caused a jump from the P state to the AP state (560 Ω) at +0.6 mA. Further increase in the pulse height followed by a reduction to zero current did not affect the state. Subsequently, negative pulses were applied to the sample. At −0.35 mA, the sample switched its magnetization from the AP state to the P state. The average switching current density was about 6×10^6 A cm^{-2}. No intermediate resistance state between the P and the AP states was observed during either of the two switching events: the switching events were always abrupt

and complete. The slope of the hysteresis loop at the switching point is only due to the discrete measurement points, which were not regularly placed because of the large change in the resistance. The P to AP and AP to P switching events occurred at different current levels because of the dipole and the so-called orange peel coupling field from the pinned layer. In the experiment, an external field of $-4.8\,\mathrm{kA\,m^{-1}}$ was applied to cancel these coupling fields.

3. Landau–Lifshitz–Gilbert equation with spin-torque terms

For simplicity, here, we assume that the local spins within the magnetic cell are aligned in parallel and form a coherent macro-spin. This assumption is not strictly valid, even in the static case, since the demagnetization field inside the cells is not uniform. Nevertheless, despite the predicted limitations, the macro-spin model is still useful because of both its transparency and its definite validity for uniform-mode (ferromagnetic resonance (FMR) mode) excitations.

The time evolution of the macro-spin, $\boldsymbol{S}_2$, can be expressed by the following Landau–Lifshitz–Gilbert (LLG) equation, which includes a spin-transfer torque term [9,10] and a field-like torque term [16–23]:

$$\frac{\mathrm{d}\boldsymbol{S}_2}{\mathrm{d}t} = \gamma \boldsymbol{S}_2 \times \boldsymbol{H}_{\mathrm{eff}}(V) + G_{\mathrm{ST}} V \boldsymbol{s}_2 \times (\boldsymbol{s}_1 \times \boldsymbol{s}_2) + G_{\mathrm{FT}} V \boldsymbol{s}_1 \times \boldsymbol{s}_2 - \alpha \boldsymbol{S}_2 \times \frac{\mathrm{d}\boldsymbol{s}_2}{\mathrm{d}t}. \tag{3.1}$$

Here $\boldsymbol{s}_2$ ($\boldsymbol{s}_1$) is a unit vector that expresses the direction of the spin angular momentum of the free layer (fixed layer); the orbital moment, which is very small for 3d transition metals, is neglected in this treatment; and γ is the gyromagnetic ratio, where $\gamma < 0$ for electrons. The first term is the effective field torque, the second is the spin-transfer torque, the third is a field-like torque and the fourth represents Gilbert damping. The effective field, $\boldsymbol{H}_{\mathrm{eff}}$, is the sum of the external, demagnetization and anisotropy fields. As will be explained later, the anisotropy field can be controlled using the applied bias voltage, V. G_{ST} and G_{FT} are coefficients of the intensity of the spin-transfer and field-like torque terms, respectively. In the final term, α is the Gilbert damping factor ($\alpha > 0$).

The directions of the torques and the trajectory during magnetization reversal are illustrated in figure 3, for the case of an elliptical MTJ. The effective field torque promotes a precession motion of $\boldsymbol{S}_2$ around the major axis of the ellipse, while the damping torque tends to reduce the opening angle of the precession. The spin-transfer torque is parallel to the damping torque and may change its sign corresponding to the sign of the current. Therefore, if we apply a large enough current having an appropriate sign, the spin-transfer torque overcomes the damping torque, resulting in negative effective damping. This negative damping results in an increase in the opening angle of the precession motion, i.e. an amplification of the precession takes place. Depending on the angular dependence of the effective damping, the amplification of the precession motion leads to a limit cycle (spin-transfer oscillation (STO)) [24] or to a total magnetization reversal (SIMS) [10,12].

In figure 3, the trajectory for the SIMS (figure 3*a*) is compared with the trajectory for the magnetic-field-induced magnetization switching (figure 3*b*). The figure also illustrates the magnetic potential shapes during switchings. In the

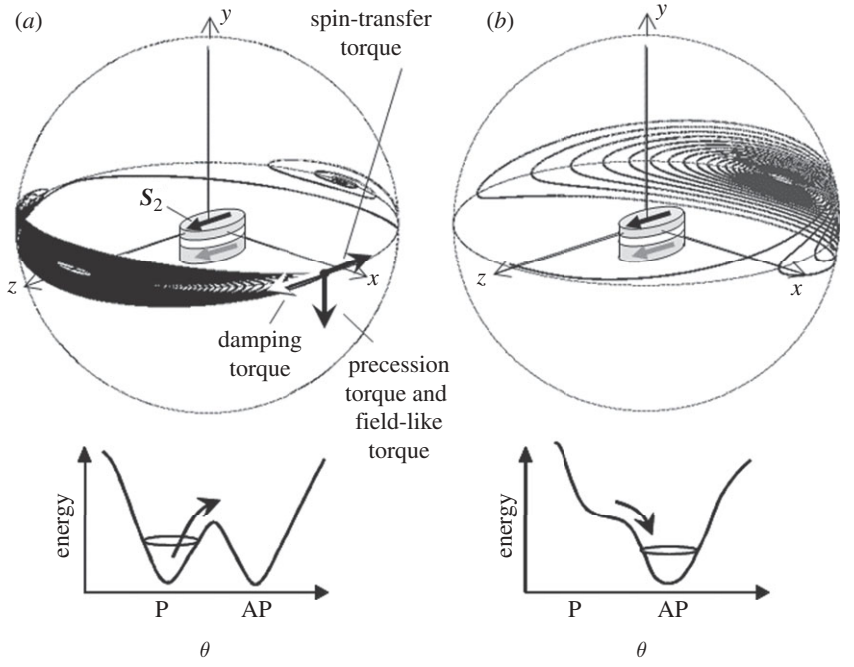

Figure 3. Comparison of the magnetization processes driven by (*a*) spin-transfer torque and (*b*) external magnetic field, for in-plane magnetized nanopillars.

absence of a current and an external magnetic field, the potential shows a double minimum for P and AP configurations of the local spin. For the particular case of SIMS, the spin-transfer torque does not affect the shape of the magnetic potential but amplifies the precession, thereby providing energy to the local spin system. Once the orbital crosses the equator, it converges rapidly to the opposite direction, since the spin-transfer torque extracts energy from the local spin system. In other words, the spin-transfer torque amplifies the precession in the front hemisphere, while enhancing the damping in the back hemisphere. In contrast to this process, the external magnetic field deforms the magnetic potential, and the minimum on the P side disappears. Therefore, the local spin turns towards the AP side. The local spin system, however, keeps excess energy in the back hemisphere. As a result, it cannot stop at once and shows precessional motion (ringing) in the back hemisphere.

4. Spin-dependent tunnelling and spin-transfer torque

Here, we obtain the expression for the spin-transfer torque according to Slonczewski's simple treatment [4,25]. A typical device structure is shown in figure 4. When current is passed through this device, the electrons are first polarized by the thick ferromagnetic layer FM1 and then injected into the thin ferromagnetic layer FM2 through the barrier. The spins of the injected electrons interact with the local spin angular momentum, $\boldsymbol{S}_2$, by exchange interaction and exert torque. If the exerted torque is large enough, the magnetization in FM2 is

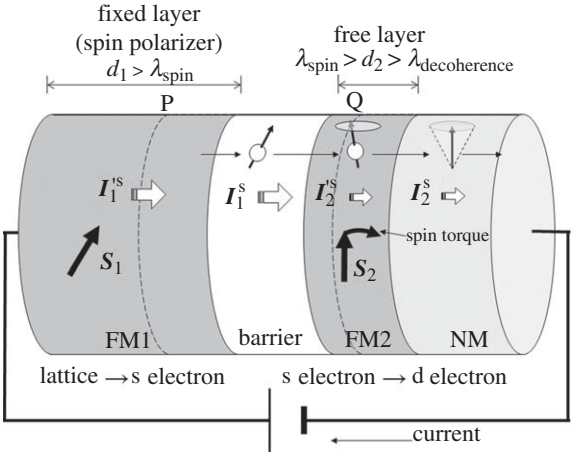

Figure 4. Schematic of a magnetic nanopillar consisting of two ferromagnetic layers separated by a barrier layer. The electrons are spin polarized by the thick ferromagnetic layer (FM1: spin polarizer) and then injected into the thin ferromagnetic layer (FM2: free layer) through the barrier layer. The injected spins undergo precession in FM2 and lose their transverse components. The lost spin components are transferred to the local spin moment in FM2. NM is a non-magnetic layer.

reversed or continuous precession is excited. As a consequence of the total spin conservation, the change in the local angular momentum is equal to the difference between the injected spin current and the gushed spin current,

$$\left(\frac{\mathrm{d}\boldsymbol{S}_2}{\mathrm{d}t}\right)_{\mathrm{ST}} = \boldsymbol{I}_1^{\mathrm{S}} - \boldsymbol{I}_2^{\mathrm{S}}, \tag{4.1}$$

where $\boldsymbol{I}_1^{\mathrm{S}}$ and $\boldsymbol{I}_2^{\mathrm{S}}$ are the spin currents at the barrier and the non-magnetic (NM) layer, respectively. Since FM2 is very thin, we neglected the spin–orbit interaction in FM2. Equation (4.1) indicates that a torque can be exerted on the local angular momentum as a result of spin transfer from the conduction electrons.

Here, we assume that FM1 is thick enough; therefore, at point P in FM1 (figure 4), the conduction spins are relaxed and aligned parallel to $\boldsymbol{S}_1$. In addition, we assume that, at point Q inside FM2, the conduction electrons have already lost their transverse spin component on average because of the decoherence mechanism and that the spins are aligned parallel to $\boldsymbol{S}_2$. Therefore, the spin currents at points P and Q, $\boldsymbol{I}_1^{'\mathrm{S}}$ and $\boldsymbol{I}_2^{'\mathrm{S}}$, respectively, are parallel to $\boldsymbol{S}_1$ and $\boldsymbol{S}_2$. We also assume the absence of spin scattering at the interfaces; therefore, $\boldsymbol{I}_j^{'\mathrm{S}} = \boldsymbol{I}_j^{\mathrm{S}}$. Since the spins of the conduction electrons at P and Q are either the majority or minority spin of the host materials, the total charge current in the MTJ can be expressed as the sum of the following four components:

$$I^{\mathrm{Q}} = I_{++}^{\mathrm{Q}} + I_{+-}^{\mathrm{Q}} + I_{-+}^{\mathrm{Q}} + I_{--}^{\mathrm{Q}}. \tag{4.2}$$

Here, suffixes + and − indicate the majority and minority spin channels, respectively. For example, I_{+-}^{Q} represents a charge current flow from the FM2 minority spin band into the FM1 majority spin band. These charge currents are

expressed using the conductance for each spin sub-channel, $G_{\pm\pm}$:

$$\left.\begin{aligned} I^{\mathrm{Q}}_{\pm\pm} &= VG_{\pm\pm}\cos^2\frac{\theta}{2} \\ \text{and}\qquad I^{\mathrm{Q}}_{\mp\pm} &= VG_{\mp\pm}\sin^2\frac{\theta}{2}. \end{aligned}\right\} \tag{4.3}$$

Here, V is the applied voltage. The angle dependence of the conductions can be derived from the fact that the spin functions in FM1 are $|\mathrm{maj.}\rangle = \cos(\theta/2)|\uparrow\rangle + \sin(\theta/2)|\downarrow\rangle$ for the majority spins and $|\mathrm{min.}\rangle = \sin(\theta/2)|\uparrow\rangle - \cos(\theta/2)|\downarrow\rangle$ for the minority spins, and those in FM2 are $|\uparrow\rangle$ and $|\downarrow\rangle$, respectively. Since the spin quantization axes at P and Q are parallel to $\boldsymbol{S}_1$ and $\boldsymbol{S}_2$, respectively, the spin currents at P and Q are obtained easily as follows:

$$\left.\begin{aligned} \boldsymbol{I}'^{\mathrm{S}}_1 &= \frac{\hbar}{2}\frac{1}{-e}(I^{\mathrm{Q}}_{++} + I^{\mathrm{Q}}_{+-} - I^{\mathrm{Q}}_{-+} - I^{\mathrm{Q}}_{--})\mathbf{e}_1 \\ \text{and}\qquad \boldsymbol{I}'^{\mathrm{S}}_2 &= \frac{\hbar}{2}\frac{1}{-e}(I^{\mathrm{Q}}_{++} - I^{\mathrm{Q}}_{+-} + I^{\mathrm{Q}}_{-+} - I^{\mathrm{Q}}_{--})\mathbf{e}_2. \end{aligned}\right\} \tag{4.4}$$

Therefore, after a straightforward calculation, the total current and spin-transfer torque are obtained as follows:

$$\left.\begin{aligned} I^{\mathrm{Q}} &= \left(\frac{G_{++}+G_{--}+G_{+-}+G_{-+}}{2} + \frac{(G_{++}+G_{--})-(G_{+-}+G_{-+})}{2}\mathbf{e}_2\cdot\mathbf{e}_1\right)V \\ &= \left(\frac{G_{\mathrm{P}}+G_{\mathrm{AP}}}{2} + \frac{G_{\mathrm{P}}-G_{\mathrm{AP}}}{2}\cos\theta\right)V \\ \text{and}\quad \left(\frac{\mathrm{d}\boldsymbol{S}_2}{\mathrm{d}t}\right)_{\mathrm{ST}} &= \frac{\hbar}{2}\frac{1}{-e}\left(\frac{G_{++}-G_{--}}{2} + \frac{G_{+-}-G_{-+}}{2}\right)(\mathbf{e}_2\times(\mathbf{e}_1\times\mathbf{e}_2))V \\ &= G_{\mathrm{ST}}(\mathbf{e}_2\times(\mathbf{e}_1\times\mathbf{e}_2))V. \end{aligned}\right\} \tag{4.5}$$

In the first equation in (4.5), the tunnel conductance is a function of $\cos\theta$. In the second equation, the spin torque is proportional to $\sin\theta$, similar to the case in equation (3.1) (note that $|\mathbf{e}_2\times(\mathbf{e}_1\times\mathbf{e}_2)| = \sin\theta$). Slonczewski termed G_{ST} as the 'torquance', which is an analogue of conductance. A particular point in the MTJs is that the spin torques may have a bias voltage dependence because $G_{\pm\pm}$ has bias voltage dependence.

5. Spin-torque diode effect and spin-torque measurements

The strong coupling between spin configuration and electrical conductivity gives rise to various nonlinear effects like spin-injection magnetization reversal and spin-transfer oscillation. The spin-torque diode effect is also such a nonlinear effect that manifests not only in MTJs but also in magnetoresistive materials in general. The effect consists of a linear excitation of magnetic resonance by spin torques and a linear electric response of the device to applied current (Ohm's law).

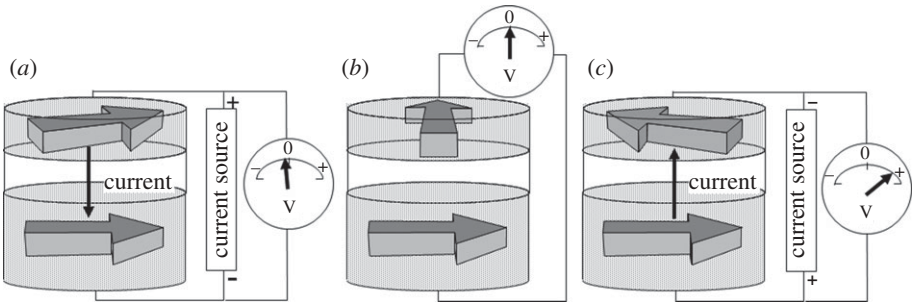

Figure 5. Schematic of the spin-torque diode effect: (*a*) negative current; (*b*) null current; and (*c*) positive current. Details are explained in the text.

To observe the spin-torque diode effect, we prepare a special nanopillar in which both free-layer and fixed-layer magnetizations are in-plane but perpendicular to each other, as shown in figure 5*b*. We then apply a negative current that induces a preferential parallel configuration of the spins. Thus, the resistance of the junction becomes smaller and we observe only a small negative voltage across the junction for a given current (figure 5*a*). Next, we apply a positive current of the same amplitude. This current induces a preferential AP configuration and the resistance becomes higher. We observe a larger positive voltage across the junction for a given current (figure 5*c*). This is the spin-torque diode effect. The effect can be large if the frequency of the applied current matches with the FMR frequency of the free layer. In other words, this effect provides a sensitive FMR measurement technique for the nanopillar moment excited by the spin torque. Therefore, the effect is useful to investigate the high-frequency dynamics of the nanopillar and the physical mechanism of the spin torque itself.

The effect can also be referred to as homodyne detection. When the radio-frequency (rf) current across the MTJ is $\delta V G(\theta)\cos\omega t$, because of the spin-transfer and field-like torques exerted on the free-layer spins (equation (3.1)), the free-layer spin oscillates at the same frequency but with a different phase. As a result, the resistance of the MTJ oscillates as $\delta R\cos(\omega t+\phi)$, which is linear in δV. Thus, from Ohm's law, the following additional voltages appear across the junction:

$$\delta R\cos(\omega t+\phi)\times\delta V G(\theta)\cos\omega t=\frac{G(\theta)}{2}\delta R\,\delta V(\cos\phi+\cos(2\omega t+\phi)). \tag{5.1}$$

Here, we see that the frequencies of the additional voltages are zero (DC) and 2ω. It means that, under spin-torque FMR excitation, the MTJs may possess a rectification function and a mixing function. Because of these new functions, Tulapurkar *et al.* [26] referred to these MTJs as spin-torque diodes and these effects as spin-torque diode effects. By observing the effect, one can determine the MTJ response to the applied rf voltage precisely with phase sensitivity.

For the spin-transfer torque, the maximum DC voltage output is obtained when the frequency of the applied rf voltage matches with the FMR frequency of the free-layer spin. An expression for the rectified DC voltage at resonance is shown

below together with that for p–n junction semiconductor diodes:

$$(V_{\mathrm{DC}})_{\max} = \begin{cases} \dfrac{1}{4}\dfrac{G_{\mathrm{P}} - G_{\mathrm{AP}}}{G_{\mathrm{P}} + G_{\mathrm{AP}}}\dfrac{\delta V^2}{V_{\mathrm{c}}} & \text{(spin-torque diode)}, \\ \dfrac{1}{4}\dfrac{\delta V^2}{k_{\mathrm{B}}T/e} & \text{(p–n junction semiconductor diode)}, \end{cases} \tag{5.2}$$

where $k_{\mathrm{B}}T/e$ is the thermal voltage (25 mV at RT). For both cases, the rectified voltage is a quadratic function of the applied rf voltage. Therefore, these detectors are referred to as quadratic detectors. The output voltage is scaled by the critical switching voltage, V_{c}, for the spin-torque diode and by $k_{\mathrm{B}}T/e$ for the p–n junction semiconductor diode. A typical critical switching voltage for the MTJs was about 300 mV and was about 10 times larger than $k_{\mathrm{B}}T/e$ for the experiments in Tulapurkar *et al.* [26]. Therefore, the output of the spin-torque diode was smaller than that of the semiconductor diode. An increase in the MR ratio and a reduction of the critical switching voltage will enhance the performance of the spin-torque diode.

Now, we introduce an application of the effect to measure the bias voltage dependences of the spin torques in the MTJs. From equation (3.1), both the spin-transfer torque and the field-like torque can excite a uniform mode (FMR mode) in the free layer. The field-like torque excites FMR in the same way the external magnetic field does, since it has the same symmetry as the external field, whereas FMR excited by the spin-transfer torque shows a 90° difference in the phase. This difference in the precessional phase is a consequence of the different directions of the respective torques (figure 3). The motion of the spin, illustrated in figure 5, corresponds to that excited by the spin-transfer torque at the resonance frequency. However, the motion of the spin excited by the field-like torque shows a 90° difference in the phase. As a consequence, only the resonance excited by the spin-transfer torque can rectify the rf current at the resonance frequency. In the frequency region, the spectrum excited by the spin-transfer torque exhibits a single bell-shaped peak centred at the resonance frequency but that excited by the field-like torque is of a dispersion type. This very clear difference provides us with an elegant method to distinguish spin-transfer torque from field-like torque [26–28]. Sankey *et al.* [27] and Kubota *et al.* [28] experimentally observed the bias dependence of the torques in CoFeB/MgO/CoFeB magnetic tunnel junctions.

In figure 6*a*, a schematic of the measurement set-up for the spin-torque diode effect with a cross-sectional view of the MTJ employed in Tulapurkar *et al.* [26] is shown. The rf voltage was applied through a bias T from a high-frequency oscillator and the DC voltages across the MTJ can be detected using a DC nanovoltmeter. In figure 6*b*, an example of the diode spectrum (filled dots) is shown together with a fitting curve. The data were taken at RT without applying a DC bias voltage. The observed spectrum has an asymmetrical shape and was well fitted as the superposition of a bell-shaped spectrum and a dispersion-shaped spectrum. By this fitting, the spectrum was decomposed into a contribution from the spin-transfer term and from the field-like term. The intensity and even the sign of the field-like term contribution varied from sample to sample, while those of the spin-transfer term were reproducible. Therefore, it is thought that the contribution from the field-like term at zero bias voltage is very sensitive to small

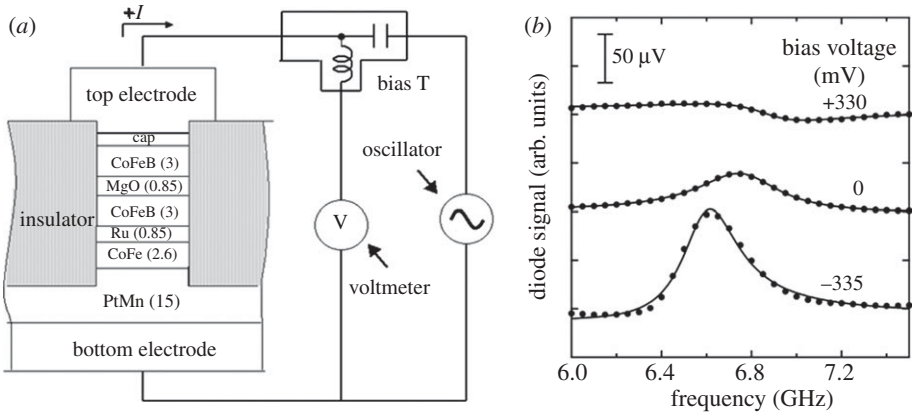

Figure 6. (*a*) Measurement set-up for the spin-torque diode effect measurements. (*b*) Spin-torque diode spectra for a CoFeB/MgO/CoFeB MTJ at RT. Data (dots) are well fitted by a theoretical curve considering contributions from both the spin-transfer torque and the field-like torque.

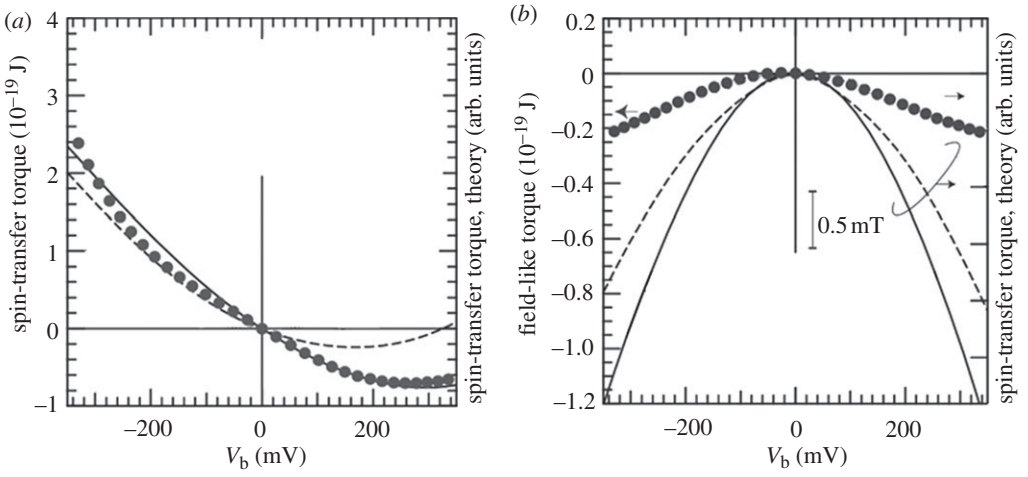

Figure 7. Bias dependence of (*a*) the spin-transfer torque and (*b*) the field-like torque. Curves were obtained by theoretical model calculations (after Theodonis *et al.* [21]) with different spin splitting, ε. Circles show the experimental results obtained for a CoFeB/MgO/CoFeB MTJ using the spin-torque diode effect (after Kubota *et al.* [28]). Circles, experiment (RT); solid line, theory, $e = 2.25$ eV; dashed line, theory, $e = 2.00$ eV.

defects in the magnetic cell. By taking a sample that does not show a contribution from the field-like term, Kubota *et al.* have investigated the DC bias voltage dependence of the spectra [28,29]. The results are shown in figure 7 together with theoretical predictions [21].

As shown in the figure, the bias dependence of the spin-transfer torque is neither monotonic nor symmetric. This slightly complicated behaviour can be understood from equation (4.5). Assume that FM1 and FM2 are made of the

same material. Then, owing to the symmetric conditions for tunnelling, the conductance $(G_{++} - G_{--})$ is an even function of the voltage but $(G_{+-} - G_{-+})$ is odd. Since the total torquance is the sum of these functions, the torquance may show somewhat complicated bias voltage dependence. The experimental data were well explained by band theory, in which bias-dependent spin sub-channel conductivities were taken into account [21].

It has been pointed out that one of the important origins of the field-like torque in MTJs is the change in the interlayer exchange coupling through the barrier layer at a finite bias voltage [20,21]. In figure 7*b*, the theoretically obtained strengths of the field-like torque are plotted as a function of the bias voltage [30]. As theoretically predicted for symmetrical MTJs, the field-like torque is an even function of the bias voltage. Its strength is less than one-fifth that of the spin-transfer torque. The experimental results obtained so far [26,27] seem to agree with this prediction.

The field-like torque could have originated from other mechanisms that are similar to those responsible for the 'β-term' in magnetic nanowires. Several mechanisms, such as spin relaxation [16,18], Gilbert damping [22], momentum transfer [19], spin-wave excitations [23] and a current-induced Ampere field, have been proposed for the origin of the 'β-term'. Further quantitative and systematic investigations on the field-like torque are necessary to reveal the intrinsic origins of the field-like torque.

6. Spin-transfer oscillator and negative resistance effect

It is known that magnetic nanopillars may show spontaneous precession under the simultaneous application of both a DC voltage and an external field [24]. The output power, however, was very small (typically in the range of several tens of picowatts) because of a small magnetoresistance effect in the metallic junctions. Since the rf output power from a spin-transfer oscillator is a quadratic function of the magnetoresistance effect, a tremendously larger output power can be expected for MTJs. For this purpose, we have developed an MTJ with very low resistance × area product and a high MR, and observed a large rf output from CoFeB/MgO/CoFeB MTJs [31].

We also predict that an MTJ with a very high MR and rf emission may also show a negative resistance effect, and thus possess an amplification function when it is driven by a constant-voltage mode under an external field. At zero external field under an applied voltage, the MTJ only shows a switching event and hysteresis in the I–V curve, whereas the I–V curve predicted for the 90 Oe external field does not show P to AP switching but a continuous and reversible transition from the P state to the precession state. During this transition, the current becomes smaller for a larger voltage, i.e. a negative differential resistance is expected. Such a negative resistance is not expected for MTJs with tunnelling magnetoresistance values smaller than 100 per cent. In semiconductor physics, it is known that, if a two-terminal device shows a negative differential resistance, it can amplify small electric signals, such as in Esaki diodes. This means that a simple MTJ is not only a passive magnetoresistance device but also an active device that shows spontaneous oscillation, negative resistance and amplification functions owing to the spin-transfer torque.

7. Surface magnetic anisotropy and voltage effect

The manipulation of the magnetization direction by an electric current has been investigated in the research field of magnetic memories and logic applications. In particular, recent findings of the spin-transfer effect, as reviewed in the previous sections, have accelerated the development of novel manipulation methods of magnetic moments in a nanoscale magnetic element. However, the current consumes a much larger energy compared with the thermal stabilization energy for magnetic bit information, which is often estimated as $(50–60) \times k_{\mathrm{B}} T$. Since the voltage, as in complementary metal–oxide–semiconductor field-effect transistor (C-MOS FET) technology, does not consume high energy, in principle, voltage control of the magnetization will be a promising candidate as a future writing technique.

There have been a lot of experimental approaches for voltage control of magnetic properties, such as the electric-field control of magnetostriction in a multi-layered stack with piezoelectric materials [32,33], Curie temperature in ferromagnetic semiconductors [34–36], voltage control of interlayer exchange coupling [37], magnetoelectric effect in single-phase multiferroic materials [38] or a two-phase multiferroic system including artificial ferroelectric/ferromagnetic heterostructures [30,39–43]. Recently, as an important pioneering work, a direct voltage application effect on magnetic anisotropy was reported in thin 3d ferromagnetic metal layers of FePt (FePd) using a liquid electrolyte [44]. However, to employ this effect in practical applications, it should be realized in all-solid-state devices. For this purpose, we employed an ultrathin Fe (001) single-crystalline film to control its surface magnetic anisotropy by voltage application [45].

The magnetic energy of an ultrathin film is expressed as a function of the film thickness, t, and its magnetization direction as follows:

$$\frac{E_{\mathrm{mag}}}{A} = \mu_0 m_2 \boldsymbol{s}_2 \cdot \boldsymbol{H}_{\mathrm{ext}} t + K_{\mathrm{volume}}(\boldsymbol{s}_2) t + K_{\mathrm{surface}}(\boldsymbol{s}_2, V), \tag{7.1}$$

where A is the cross-sectional area of the magnetic cell, m_2 is the magnetization in the magnetic cell, $\boldsymbol{H}_{\mathrm{ext}}$ is the applied external field, and $\mu_0 = 4\pi \times 10^{-7}\,\mathrm{H\,m^{-1}}$ is the magnetic susceptibility of the vacuum. $K_{\mathrm{volume}}(\boldsymbol{s}_2)$ is the crystalline anisotropy energy per unit volume in the magnetic cell and is dependent on the direction of the spin, $\boldsymbol{s}_2$, reflecting the crystalline symmetry. $K_{\mathrm{surface}}(\boldsymbol{s}_2, V)$ is the surface magnetic anisotropy energy per unit surface area. This term arises from broken symmetry at the surface and can be changed by a voltage application. From $\boldsymbol{s}_2$, the dependence of the magnetic energy, the effective magnetic field, $\boldsymbol{H}_{\mathrm{eff}}$, in equation (3.1) is obtained as follows:

$$\boldsymbol{H}_{\mathrm{eff}} = \frac{1}{\mu_0 A\, t\, m_2} \frac{\partial E_{\mathrm{mag}}}{\partial \hat{s}_2}. \tag{7.2}$$

Bruno treated the surface magnetic anisotropy in 3d ferromagnetic metals taking spin–orbit interaction as a perturbation [46]. Among d-bands, d_{xz}, d_{yz}, d_{xy} and $\mathrm{d}_{x^2-y^2}$ bands contribute to the perpendicular magnetic anisotropy [47]. By using

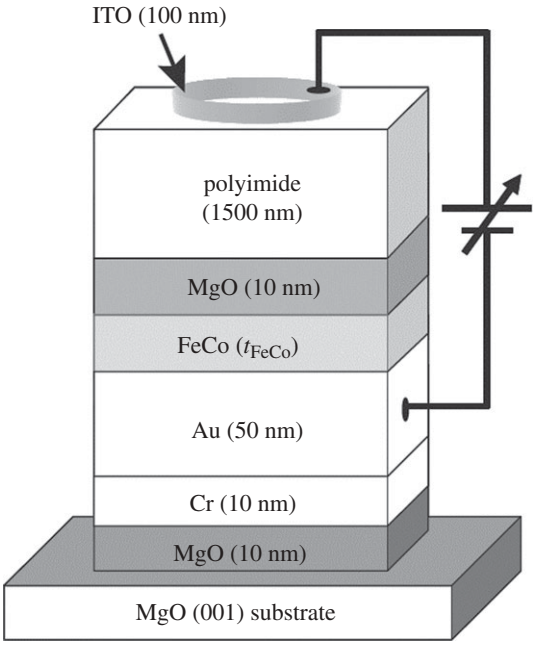

Figure 8. Schematic of the sample stack.

a fourfold rotation operator around the y-axis, $\tilde{C}_{4y}$, Bruno's expression (eqn (12) in Bruno [46]) is simplified and the change in the magnetic energy between perpendicular magnetization and in-plane magnetization is expressed as follows:

$$\Delta E_{\mathrm{mag}} = -\frac{\xi^2}{4}(1-\tilde{C}_{4y}) \sum_{\substack{\varepsilon_n<\varepsilon_{\mathrm{F}} \\ \varepsilon_{n'}>\varepsilon_{\mathrm{F}}}} \frac{\sigma_n \sigma_{n'}}{\varepsilon_{n'}-\varepsilon_n} \delta_{\boldsymbol{k}_n \boldsymbol{k}_{n'}} \left| \begin{array}{l} \langle n|\mathrm{d}_{yz}\rangle\langle \mathrm{d}_{zx}|n'\rangle - \langle n|\mathrm{d}_{zx}\rangle\langle \mathrm{d}_{yz}|n'\rangle \\ \quad + 2\langle \mathrm{d}_{xy}|n\rangle\langle n'|\mathrm{d}_{x^2-y^2}\rangle \\ \quad - 2\langle \mathrm{d}_{x^2-y^2}|n\rangle\langle n'|\mathrm{d}_{xy}\rangle \end{array} \right|^2, \quad (7.3)$$

where n and n' represent electronic states below and above the Fermi level, ε_{F}, respectively, ξ is the spin–orbit parameter [46], ε_n, $\boldsymbol{k}_n$ and $\boldsymbol{\sigma}_n$ are single electron state energy, wavevector and spin of the state n, respectively, and $\tilde{C}_{4y}$ operates upon the d-state base functions and rotates the atomic orbital part as $\tilde{C}_{4y}|\mathrm{d}_{yz}\rangle = |\mathrm{d}_{xy}\rangle$. In the ultrathin Fe (001) layer, since the majority spin d-bands are almost occupied [48], the minority spin d-bands mainly contribute to the surface anisotropy energy. The wave functions and their eigen-energies are perturbed by a voltage application as follows:

$$\left.\begin{array}{rl} |n\rangle = |n^{(0)}\rangle + \displaystyle\sum_{n'\neq n} \frac{\langle n'^{(0)}| - e\phi(\boldsymbol{x})|n^{(0)}\rangle}{\varepsilon_n^{(0)} - \varepsilon_{n'}^{(0)}} |n'^{(0)}\rangle & \\ \text{and} \qquad \varepsilon_n = \varepsilon_n^{(0)} + \langle n^{(0)}| - e\phi(\boldsymbol{x})|n^{(0)}\rangle, & \end{array}\right\} \quad (7.4)$$

where $\phi(\boldsymbol{x})$ is a self-consistent scalar potential.

The application of a voltage between ferromagnetic ultrathin electrodes deposited onto a metal substrate and a metal counterelectrode that is separated by an insulator (figure 8) provides an electric field and potential, which penetrate into the metal surface. The penetration depth, λ, estimated from the density of states at the Fermi energy in Fe is about one-sixth of the atomic layer distance, d ($d = 0.143$ nm for the Fe (001) surface). The electric potential around the topmost atomic layer is estimated to be

$$\phi(z) = -\lambda E_0 \mathrm{e}^{(z-d/2)/\lambda} = -\lambda E_0 \mathrm{e}^{(-d/2)/\lambda}\left(1 + \frac{z}{\lambda} + \frac{1}{2}\left(\frac{z}{\lambda}\right)^2 + \cdots\right) \tag{7.5}$$

for a classic jellium model. Here, z is a coordinate that is perpendicular to the film surface. The origin is at the centre of the topmost atomic layer. E_0 is the electric field strength at the surface ($z = d/2$). The energy shift of the 3d m orbital can be expressed using a Taylor expansion of the potential around an atomic position as

$$\delta\varepsilon_{\perp,mm} = \langle m| - e\phi|m\rangle \cong e\lambda E_0 \mathrm{e}^{(-d/2)/\lambda}\left(1 + \frac{1}{2\lambda^2}\frac{1}{3}\left(\langle Q_{zz}\rangle_m + \langle r^2\rangle\right) + \cdots\right), \tag{7.6}$$

with $\langle Q_{zz}\rangle_m$ being the quadrupole tensor element and $\langle r^2\rangle \cong (d/2)^2$ being the expectation value of the 3d orbital radius squared. The quadrupole moment depends on the magnetic quantum number m and for the 3d orbital is $\langle Q_{zz}\rangle_m = 2(2 - m^2)\langle r^2\rangle/7$. The linear term in equation (7.5) also gives an energy level shift through second-order perturbation. This Stark effect was also discussed as a candidate to control magnetic anisotropy [49]. The effect, however, is thought to be small since it is a second-order effect. In addition, this mechanism should show an even effect with respect to the applied voltage and does not agree with our observations. Therefore, in equation (7.6), the Stark effect is neglected. From equation (7.6), we estimate that $\delta\varepsilon_{\perp,mm} = 3.9, 3.4$ and 1.9 meV for $m = 0$, 1 and 2, respectively, under an electric field of $1\,\mathrm{V\,nm^{-1}}$ at the surface. Such an orbit-dependent energy shift causes a first-order change in the anisotropy energy as follows:

$$\Delta E_{\mathrm{mag}} \cong -\xi^2 \frac{1}{4} \sum_{\substack{\boldsymbol{k},n,n' \\ \varepsilon_{n,\downarrow} < \varepsilon_{\mathrm{F}} \\ \varepsilon_{m,\downarrow} > \varepsilon_{\mathrm{F}}}} \frac{\begin{array}{l}|\langle n|\mathrm{d}_{yz}\rangle\langle \mathrm{d}_{zx}|n'\rangle|^2(\delta\varepsilon_{\perp,nn} - \delta\varepsilon_{//,nn}) \\ +|\langle n|\mathrm{d}_{zx}\rangle\langle \mathrm{d}_{yz}|n'\rangle|^2(\delta\varepsilon_{\perp,n'n'} - \delta\varepsilon_{//,n'n'})\end{array}}{(\varepsilon_{\boldsymbol{k},n'} - \varepsilon_{\boldsymbol{k},n})^2}, \tag{7.7}$$

where $\delta\varepsilon_{//,nn}$ is the virtual energy shift with the electric field applied along the x-direction. In the above expression, the contributions from the d_{xy} and $\mathrm{d}_{x^2-y^2}$ orbitals are neglected for simplicity. Accumulation and depletion of the electrons at the surface also contribute to the magnetic anisotropy energy change if the system has a large magnetic anisotropy without voltage application. This is usually true since the surface provides a broken symmetry and surface magnetic anisotropy. Finally, a change in the wave function by voltage also causes magnetic anisotropy change if two bands include the same d-orbital, since the matrix element $\langle n'^{(0)}| - e\phi(\boldsymbol{x})|n^{(0)}\rangle$ is zero for different d-orbitals.

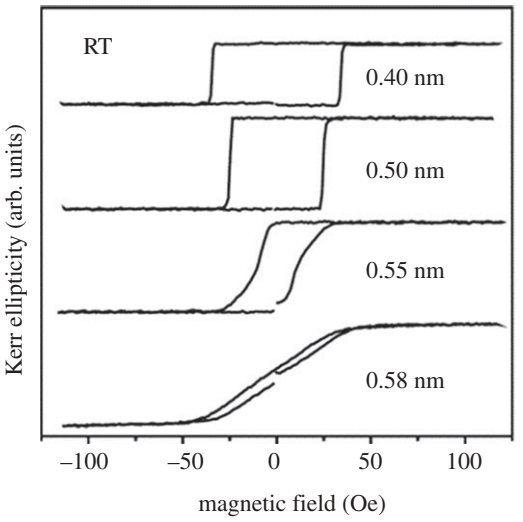

Figure 9. Thickness dependence of magnetic hysteresis curves of the ultrathin FeCo layer sandwiched between Au and MgO layers. Magnetic fields were applied perpendicular to the film plane.

8. Voltage control of magnetic anisotropy in ultrathin 3d ferromagnetic layer/MgO junctions

We have succeeded in observing a large voltage-induced perpendicular magnetic anisotropy change in the ultrathin FeCo layer and demonstrated a voltage-induced magnetization switching by assisting magnetic fields in an all-solid-state device at RT [45,50]. The schematic of the sample stack is shown in figure 8. Multilayers of MgO (10 nm)/Cr (10 nm)/Au (50 nm)/$Fe_{80}Co_{20}$ (t_{FeCo})/MgO (10 nm) were grown on a single-crystal MgO (001) substrate by molecular beam epitaxy. To improve the surface flatness, an Au buffer layer was annealed at 200°C after RT deposition. The ultrathin FeCo and MgO layers were epitaxially grown on the Au layer at RT. After depositing the top MgO layer, the sample was removed from the deposition chamber and the surface was coated with a polyimide layer (1500 nm in thickness) by using a spin coater. An indium tin oxide (ITO) electrode of 1 mm diameter was fabricated using a metal mask. The bias voltage, V_{bias}, was applied between the top ITO electrode and the bottom Au electrode. The polyimide layer was used to assure a pinhole-free barrier over an extended area. The bias direction was defined with respect to the top ITO electrode (figure 8). To investigate the magnetic hysteresis curve of the FeCo layer, the Kerr ellipticity, η_K, was measured in the polar configuration under the application of voltage.

Figure 9 shows representative magnetic hysteresis curves of the ultrathin FeCo layer with different thicknesses under zero bias voltage application. The ultrathin FeCo layer, sandwiched between the Au and MgO layers, exhibits perpendicular magnetic anisotropy. The transition of the easy axis from in-plane to out-of-plane directions occurs at $t_{FeCo} = 0.58$ nm.

At around the critical thickness, the change in the hysteresis curve is expected to be the most sensitive to the voltage application. In fact, a drastic change in the hysteresis was found under bias voltage applications, as shown in figure 10. When positive V_{bias} is applied, perpendicular magnetic anisotropy is suppressed and

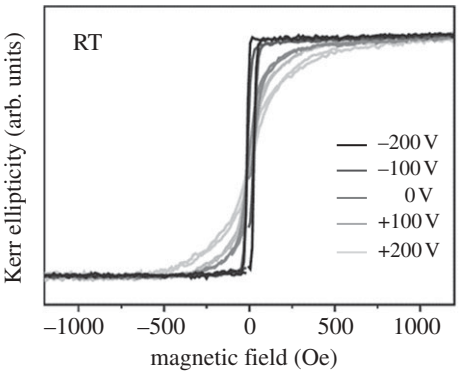

Figure 10. Magnetic hysteresis curves of a 0.58 nm thick FeCo layer, measured under various applied bias voltages.

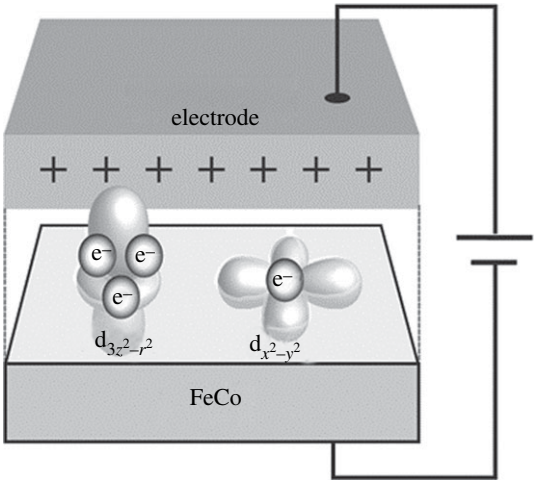

Figure 11. Schematic of the voltage-induced magnetic anisotropy change.

the saturation field increases with increasing V_{bias}. On the other hand, negative V_{bias} application induces perpendicular magnetic anisotropy. Surprisingly, clear square hysteresis, which means that the film was magnetized in the perpendicular direction, was observed under $V_{\mathrm{bias}} = -200\,\mathrm{V}$. This indicates that the electrical manipulation of the magnetic easy axis between the in-plane and out-of-plane directions was realized in this experiment.

Although the origin of this kind of direct voltage-induced magnetic anisotropy change in an ultrathin metal ferromagnetic layer is still under discussion [51–55], one possible cause is the relative change of occupation states in each 3d orbital with different orbital angular momenta by charges accumulated at the ultrathin FeCo/MgO interface (see schematic in figure 11), as pointed out in the previous section.

In the thinner region below the critical thickness, a voltage-induced anisotropy change can be observed as a change in coercivity. Figure 12*a* shows hysteresis curves measured under $V_{\mathrm{bias}} = \pm 200\,\mathrm{V}$ for the sample with $t_{\mathrm{FeCo}} = 0.48\,\mathrm{nm}$.

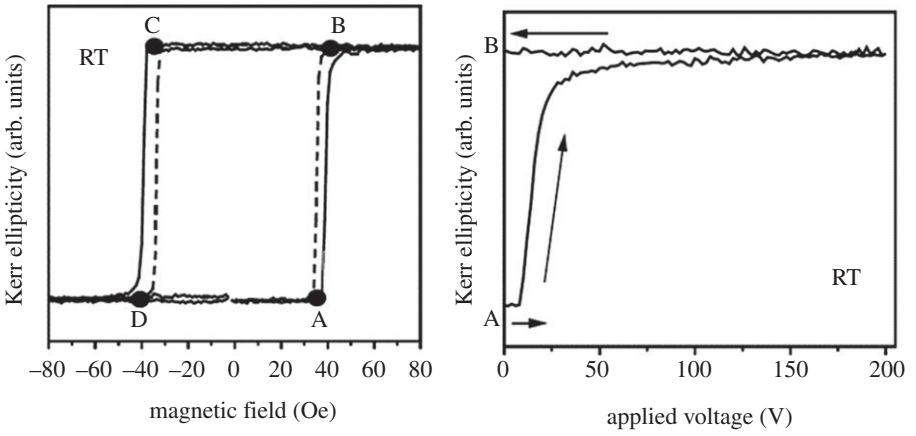

Figure 12. (*a*) Magnetic hysteresis curves of a 0.48 nm thick FeCo layer measured under bias voltages of ±200 V. Solid line, −200 V; dashed line, +200 V. (*b*) Voltage-induced magnetization switching from the A state to the B state under an assisting magnetic field of 37 Oe.

A coercivity change of about 4 Oe was induced between +200 and −200 V. Using this effect, we have demonstrated voltage-induced magnetization switching under small external magnetic fields. For example, by applying a negative saturation magnetic field of −100 Oe, followed by increasing the external magnetic field to just below the positive coercivity, the magnetization state settled in the A state in figure 12*a*. This state is stable under zero bias voltage (not shown here). However, it would be unstable under a positive voltage application owing to the decrease in the perpendicular magnetic anisotropy. Consequently, voltage application induces the magnetization to switch from the A state to the B state, as shown in figure 12*b*. Once the magnetization has switched, it remains in that state, even if we applied a negative voltage, which should increase the coercivity. Switching in the opposite direction, from the C to the D state, could also be realized under negative assisting magnetic fields by applying a positive bias voltage (not shown here). Although a similar demonstration was reported in a ferromagnetic semiconductor system [35], it should be emphasized that we could realize it in a conventional 3d ferromagnetic metal/MgO-based junction at RT. This is important progress for practical spintronic applications.

In the last part of this section, we suggest a novel magnetization switching technique, employing the voltage-induced magnetic anisotropy change found in this study. Figure 13 shows the result of the macro-spin model simulation using equation (3.1) with voltage control of the anisotropy field. Here, we used parameters obtained in our previous experiments [45]: damping constant $\alpha = 0.025$, and perpendicular magnetic anisotropy field of 150 Oe under the negative voltage application and 275 Oe under the zero bias state. The magnetic cell is assumed to have a rectangular shape, with a 200 Oe in-plane hard axis demagnetization field. An external magnetic field of 100 Oe is applied perpendicular to the film plane to tilt the magnetization towards the perpendicular direction. Under the zero bias voltage, point A is the stable state. If we apply a negative bias voltage with a slow rise time, voltage-induced anisotropy change causes the tilt of the magnetization from point A to point B. However, if the rise time of the pulse is short enough (less than 1 ns), dynamic precession and

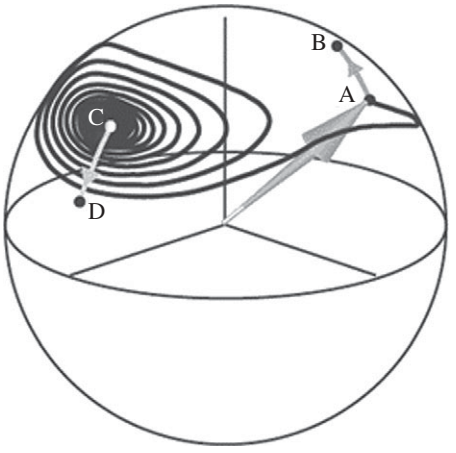

Figure 13. Macro-spin model simulation of voltage-induced dynamic magnetization switching. The grey line indicates the trajectory of the spin.

switching to another energetically stable point, C, can be achieved. When the voltage pulse is switched off with a slow fall time, the magnetization stabilizes at point D after the relaxation process. This simulation clearly shows that, if we fabricate an MgO-based junction with rf signal access, successful magnetization switching by the application of a high-speed pulse should be possible. Very recently, a similar suggestion of dynamic switching was suggested by Stöhr *et al.* [49]. Since we have already succeeded in controlling the magnetic easy axis between the out-of-plane and in-plane directions in the FeCo–MgO system, as shown in figure 10, we believe that this novel dynamic magnetization switching will be demonstrated in the near future and will be the most successful technique in combination with magnetoresistive structures.

In summary, we have succeeded in observing large voltage-induced magnetic anisotropy change in Au/ultrathin FeCo–MgO junctions. At around the critical thickness of perpendicular magnetic anisotropy in the ultrathin FeCo layer, the transition of the magnetic easy axis from the in-plane to the out-of-plane direction could be achieved. Furthermore, below the critical thickness region, the coercivity of the perpendicularly magnetized FeCo layer could be controlled by voltage application. Using this effect, we demonstrated voltage-induced magnetization switching under small external magnetic fields. We also proposed the novel magnetization switching method using dynamic precession induced by the voltage application. Our results have great significance from the viewpoint that we can control magnetic anisotropy in conventional 3d ferromagnetic metal–MgO junctions, which can be combined with high-quality Fe/MgO/Fe MTJs, leading to great innovations in ultra-low-power spintronic devices.

9. Summary

The control of the magnetization in magnetic nanodevices was discussed. Current injection into the magnetic multi-layer causes spin-transfer torque and field-like torque and yields magnetization reversal and/or spin-transfer oscillation of the thin magnetic cell. By employing a magnetic tunnel junction with the giant

tunnelling magnetoresistance effect, the spin-transfer oscillation offers a high rf power output from a nanoscale magnetic junction and the rectification effect of the rf signal. The negative resistance effect and accompanying amplification function of the magnetic tunnel junction are also predicted.

The voltage application onto the magnetic tunnel junction causes a change in magnetic anisotropy. The effect can be used as a new method for reverse magnetization with ultra-low power consumption.

We would like to acknowledge H. Maehara (Canon ANELVA); A. Fukushima and S. Yuasa (AIST); K. Konishi, Y. Shiota, T. Maruyama and A. Deac (Osaka University); and K. Tsunekawa, D. D. Djayaprawira and N. Watanabe (Canon ANELVA) for their collaborations. This study was partly supported by the New Energy and Industrial Technology Development Organization (NEDO); the G-COE programme, MEXT; and the SCOPE, MIC.

References

1 Baibich, M. N., Broto, J. M., Fert, A., Nguyen Van Dau, F., Etienne, P., Creuzet, G., Friederich, A. & Chazelas, J. 1988 Giant magnetoresistance of (001)Fe/(001)Cr magnetic superlattices. *Phys. Rev. Lett.* **61**, 2472–2475. (doi:10.1103/PhysRevLett.61.2472)

2 Miyazaki, T. & Tezuka, N. 1995 Giant magnetic tunneling effect in Fe/Al_2O_3/Fe junction. *J. Magn. Magn. Mater.* **139**, L231–L234. (doi:10.1016/0304-8853(95)90001-2)

3 Moodera, J. S. & Mathon, G. 1999 Spin polarized tunneling in ferromagnetic junctions. *J. Magn. Magn. Mater.* **200**, 248–273. (doi:10.1016/S0304-8853(99)00515-6)

4 Slonczewski, J. C. 1989 Conductance and exchange coupling of two ferromagnets separated by a tunneling barrier. *Phys. Rev. B* **39**, 6995–7002. (doi:10.1103/PhysRevB.39.6995)

5 Yuasa, S., Fukushima, A., Nagahama, T., Ando, K. & Suzuki, Y. 2004 High tunnel magnetoresistance at room temperature in fully epitaxial Fe/MgO/Fe tunnel junctions due to coherent spin-polarized tunneling. *Jpn. J. Appl. Phys.* **43**, L588–L590. (doi:10.1143/JJAP.43.L588)

6 Yuasa, S., Nagahama, T., Fukushima, A., Suzuki, Y. & Ando, K. 2004 Giant room-temperature magnetoresistance in single-crystal Fe/MgO/Fe magnetic tunnel junctions. *Nat. Mater.* **3**, 868–871. (doi:10.1038/nmat1257)

7 Parkin, S. S. P., Kaiser, C., Panchula, A., Rice, P. M., Hughes, B., Samant, M. & Yang, S. H. 2004 Giant tunnelling magnetoresistance at room temperature with MgO (100) tunnel barriers. *Nat. Mater.* **3**, 862–867. (doi:10.1038/nmat1256)

8 Jiang, L., Naganuma, H., Oogane, M. & Ando, Y. 2009 Large tunnel magnetoresistance of 1056% at room temperature in MgO based double barrier magnetic tunnel junction. *Appl. Phys. Express* **2**, 083002. (doi:10.1143/APEX.2.083002) [Retraced paper: see *Appl. Phys. Express* **4**, 019201 (2011). (doi:10.1143/APEX.4.019201)]

9 Berger, L. 1996 Emission of spin waves by a magnetic multilayer traversed by a current. *Phys. Rev. B* **54**, 9353–9358. (doi:10.1103/PhysRevB.54.9353)

10 Slonczewski, J. C. 1996 Current-driven excitation of magnetic multilayers. *J. Magn. Magn. Mater.* **159**, L1–L2. (doi:10.1016/0304-8853(96)00062-5)

11 Tsoi, M., Jansen, A. G. M., Bass, J., Chiang, W. C., Seck, M., Tsoi, V. & Wyder, P. 1998 Excitation of a magnetic multilayer by an electric current. *Phys. Rev. Lett.* **80**, 4281–4284. (doi:10.1103/PhysRevLett.80.4281) [Erratum in *Phys. Rev. Lett.* **81**, 493 (1998). (doi:10.1103/PhysRevLett.81.493)].

12 Myers, E. B., Ralph, D. C., Katine, J. A., Louie, R. N. & Buhrman, R. A. 2000 Current-induced switching of domains in magnetic multilayer devices. *Science* **285**, 867–870. (doi:10.1126/science.285.5429.867)

13 Huai, Y. M., Albert, F., Nguyen, P., Pakala, M. & Valet, T. 2004 Observation of spin-transfer switching in deep submicron-sized and low-resistance magnetic tunnel junctions. *Appl. Phys. Lett.* **84**, 3118–3120. (doi:10.1063/1.1707228)

14 Kubota, H. *et al.* 2005 Evaluation of spin-transfer switching in CoFeB/MgO/CoFeB magnetic tunnel junctions. *Jpn. J. Appl. Phys.* **44**, L1237–L1240. (doi:10.1143/JJAP.44.L1237)

15 Diao, Z., Apalkov, D., Pakala, M., Ding, Y. F., Panchula, A. & Huai, Y. M. 2005 Spin transfer switching and spin polarization in magnetic tunnel junctions with MgO and AlO_x barriers. *Appl. Phys. Lett.* **87**, 232502. (doi:10.1063/1.2139849)

16 Zhang, S. & Li, Z. 2004 Roles of nonequilibrium conduction electrons on the magnetization dynamics of ferromagnets. *Phys. Rev. Lett.* **93**, 127204. (doi:10.1103/PhysRevLett.93.127204)

17 Thiaville, A., Nakatani, Y., Miltat, J. & Suzuki, Y. 2005 Micromagnetic understanding of current-driven domain wall motion in patterned nanowires. *Europhys. Lett.* **69**, 990–996. (doi:10.1209/epl/i2004-10452-6)

18 Kohno, H., Tatara, G. & Shibata, J. 2006 Microscopic calculation of spin torques in disordered ferromagnets. *J. Phys. Soc. Jpn* **75**, 113706. (doi:10.1143/JPSJ.75.113706)

19 Tatara, G. & Kohno, H. 2004 Theory of current-driven domain wall motion: spin transfer versus momentum transfer. *Phys. Rev. Lett.* **92**, 086601. (doi:10.1103/PhysRevLett.92.086601)

20 Edwards, D. M., Federici, F., Mathon, J. & Umerski, A. 2005 Self-consistent theory of current-induced switching of magnetization. *Phys. Rev. B* **71**, 054407. (doi:10.1103/PhysRevB.71.054407)

21 Theodonis, I., Kioussis, N., Kalitsov, A., Chshiev, M. & Butler, W. H. 2006 Anomalous bias dependence of spin torque in magnetic tunnel junctions. *Phys. Rev. Lett.* **97**, 237205. (doi:10.1103/PhysRevLett.97.237205)

22 Barnes, S. E. & Maekawa, S. 2005 Current–spin coupling for ferromagnetic domain walls in fine wires. *Phys. Rev. Lett.* **95**, 107204. (doi:10.1103/PhysRevLett.95.107204)

23 Li, Z., Zhang, S., Diao, Z., Ding, Y., Tang, X., Apalkov, D. M., Yang, Z., Kawabata, K. & Huai, Y. 2008 Perpendicular spin torques in magnetic tunnel junctions. *Phys. Rev. Lett.* **100**, 246602. (doi:10.1103/PhysRevLett.100.246602)

24 Kiselev, S. I., Sankey, J. C., Krivorotov, I. N., Emley, N. C., Schoelkopf, R. J., Buhrman, R. A. & Ralph, D. C. 2003 Microwave oscillations of a nanomagnet driven by a spin-polarized current. *Nature* **425**, 380–383. (doi:10.1038/nature01967)

25 Slonczewski, J. C. 2005 Currents, torques, and polarization factors in magnetic tunnel junctions. *Phys. Rev. B* **71**, 024411. (doi:10.1103/PhysRevB.71.024411)

26 Tulapurkar, A. A., Suzuki, Y., Fukushima, A., Kubota, H., Maehara, H., Tsunekawa, K., Djayaprawira, D. D., Watanabe, N. & Yuasa, S. 2005 Spin-torque diode effect in magnetic tunnel junctions. *Nature* **438**, 339–342. (doi:10.1038/nature04207)

27 Sankey, J. C., Cui, Y. T., Sun, J. Z., Slonczewski, J. C., Buhrman, R. A. & Ralph, D. C. 2008 Measurement of the spin-transfer-torque vector in magnetic tunnel junctions. *Nat. Phys.* **4**, 67–71. (doi:10.1038/nphys783)

28 Kubota, H. *et al.* 2008 Quantitative measurement of voltage dependence of spin-transfer torque in MgO-based magnetic tunnel junctions. *Nat. Phys.* **4**, 37–41. (doi:10.1038/nphys784)

29 Suzuki, Y. & Kubota, H. 2008 Spin-torque diode effect and its application. *J. Phys. Soc. Jpn* **77**, 031002. (doi:10.1143/JPSJ.77.031002)

30 Sahoo, S., Polisetty, S., Duan, C. G., Jaswal, S. S., Tsymbal, E. Y. & Binek, C. 2007 Ferroelectric control of magnetism in $BaTiO_3$/Fe heterostructures via interface strain coupling. *Phys. Rev. B* **76**, 092108. (doi:10.1103/PhysRevB.76.092108)

31 Deac, A. M. *et al.* 2008 Bias-driven high-power microwave emission from MgO-based tunnel magnetoresistance devices. *Nat. Phys.* **4**, 803–809. (doi:10.1038/nphys1036)

32 Novosad, V., Otani, Y., Ohsawa, A., Kim, S. G., Fukamichi, K., Koike, J., Maruyama, K., Kitakami, O. & Shimada, Y. 2000 Novel magnetostrictive memory device. *J. Appl. Phys.* **87**, 6400–6402. (doi:10.1063/1.372719)

33 Overby, M., Chernyshov, A., Rokhinson, L. P., Liu, X. & Furdyna, J. K. 2008 GaMnAs-based hybrid multiferroic memory device. *Appl. Phys. Lett.* **92**, 192501. (doi:10.1063/1.2917481)

34 Ohno, H., Chiba, D., Matsukura, F., Omiya, T., Abe, E., Dietl, T., Ohno, Y. & Ohtani, K. 2000 Electric-field control of ferromagnetism. *Nature* **408**, 944–946. (doi:10.1038/35050040)

35 Chiba, D., Yamanouchi, M., Matsukura, F. & Ohno, H. 2003 Electrical manipulation of magnetization reversal in a ferromagnetic semiconductor. *Science* **301**, 943–945. (doi:10.1126/science.1086608)

36 Stolichnov, I. *et al.* 2008 Non-volatile ferroelectric control of ferromagnetism in (Ga, Mn)As. *Nat. Mater.* **7**, 464–467. (doi:10.1038/nmat2185)

37 You, C. Y. & Bader, S. D. 1999 Prediction of switching rotation of the magnetization direction with applied voltage in a controllable interlayer exchange coupled system. *J. Magn. Magn. Mater.* **195**, 488–500. (doi:10.1016/S0304-8853(99)00233-4)

38 Eerenstein, W., Mathur, N. D. & Scott, J. F. 2006 Multiferroic and magnetoelectric materials. *Nature* **442**, 759–765. (doi:10.1038/nature05023)

39 Borisov, P., Hochstrat, A., Chen, X., Kleemann, W. & Binek, C. 2005 Magnetoelectric switching of exchange bias. *Phys. Rev. Lett.* **94**, 117203. (doi:10.1103/PhysRevLett.94.117203)

40 Zavaliche, F., Zhao, T., Zheng, H., Straub, F., Cruz, M. P., Yang, P. L., Hao, D. & Ramesh, R. 2007 Electrically assisted magnetic recording in multiferroic nanostructures. *Nano Lett.* **7**, 1586–1590. (doi:10.1021/nl070465o)

41 Eerenstein, W., Wiora, M., Prieto, J. L., Scott, J. F. & Mathur, N. D. 2007 Giant sharp and persistent converse magnetoelectric effects in multiferroic epitaxial heterostructures. *Nat. Mater.* **6**, 348–351. (doi:10.1038/nmat1886)

42 Chu, Y. H. *et al.* 2008 Electric-field control of local ferromagnetism using a magnetoelectric multiferroic. *Nat. Mater.* **7**, 478–482. (doi:10.1038/nmat2184)

43 Duan, C. G., Jaswal, S. S. & Tsymbal, E. Y. 2006 Predicted magnetoelectric effect in Fe/$BaTiO_3$ multilayers: ferroelectric control of magnetism. *Phys. Rev. Lett.* **97**, 047201. (doi:10.1103/PhysRevLett.97.047201)

44 Weisheit, M., Fahler, S., Marty, A., Souche, Y., Poinsignon, C. & Givord, D. 2007 Electric field-induced modification of magnetism in thin-film ferromagnets. *Science* **315**, 349–351. (doi:10.1126/science.1136629)

45 Maruyama, T. *et al.* 2009 Large voltage-induced magnetic anisotropy change in a few atomic layers of iron. *Nat. Nanotechnol.* **4**, 158–161. (doi:10.1038/nnano.2008.406)

46 Bruno, P. 1989 Tight-binding approach to the orbital magnetic moment and magnetocrystalline anisotropy of transition-metal monolayers. *Phys. Rev. B* **39**, 865–868. (doi:10.1103/PhysRevB.39.865)

47 Kyuno, K., Ha, J.-G., Yamamoto, R. & Asano, S. 1996 First-principles calculation of the magnetic anisotropy energies of Ag/Fe(001) and Au/Fe(001) multilayers. *J. Phys. Soc. Jpn* **65**, 1334–1339. (doi:10.1143/JPSJ.65.1334)

48 Li, C., Freeman, A. J., Jansen, H. J. F. & Fu, C. L. 1990 Magnetic anisotropy in low-dimensional ferromagnetic systems: Fe monolayers on Ag(001), Au(001), and Pd(001) substrates. *Phys. Rev. B* **42**, 5433–5442. (doi:10.1103/PhysRevB.42.5433)

49 Stöhr, J., Siegmann, H. C., Kashuba, A. & Gamble, S. J. 2009 Magnetization switching without charge or spin currents. *Appl. Phys. Lett.* **94**, 072504. (doi:10.1063/1.3081421)

50 Shiota, Y., Maruyama, T., Nozaki, T., Shinjo, T., Shiraishi, M. & Suzuki, Y. 2009 Voltage-assisted magnetization switching in ultrathin $Fe_{80}Co_{20}$ alloy layers. *Appl. Phys. Express* **2**, 063001. (doi:10.1143/APEX.2.063001)

51 Nie, X. & Blügel, S. 2000 Elektrisches Feld zur Ummagnetisierung eines dünnen Films. Patentiert am Patentamt München, Amtl.Az. 19841034.4. Eur. Parl. no. 1099217.

52 Duan, C. G., Velev, J. P., Sabirianov, R. F., Zhu, Z. Q., Chu, J. H., Jaswal, S. S. & Tsymbal, E. Y. 2008 Surface magnetoelectric effect in ferromagnetic metal films. *Phys. Rev. Lett.* **101**, 137201. (doi:10.1103/PhysRevLett.101.137201)

53 Tsujikawa, M. & Oda, T. 2009 Finite electric field effects in the large perpendicular magnetic anisotropy surface Pt/Fe/Pt(001): a first-principles study. *Phys. Rev. Lett.* **102**, 247203. (doi:10.1103/PhysRevLett.102.247203)

54 Nakamura, K., Shimabukuro, R., Fujiwara, Y., Akiyama, T., Ito, T. & Freeman, A. J. 2009 Giant modification of the magnetocrystalline anisotropy in transition-metal monolayers by an external electric field. *Phys. Rev. Lett.* **102**, 187201. (doi:10.1103/PhysRevLett.102.187201)

55 Zhang, H. B., Richter, M., Koepernik, K., Opahle, I., Tasnadi, F. & Eschrig, H. 2009 Electric-field control of surface magnetic anisotropy: a density functional approach. *New J. Phys.* **11**, 043007. (doi:10.1088/1367-2630/11/4/043007)